Sigma J Eng Nat Sci, Vol. 43, No. 2, pp. 429–440, April, 2025

Sigma Journal of Engineering and Natural Sciences
Web page info: https://sigma.yildiz.edu.tr
DOI: 10.14744/sigma.2025.00034

Research Article

MHD upper-convected maxwell hybrid nano fluid over a stretching sheet: A numerical approach

G. THİRUPATHİ[1], K. GOVARDHAN[2], G. NAGARAJU[3,*], Santoshi MİSRA[4]

[1]Department of Mathematics, Rajiv Gandhi University of Knowledge Technologies, Basar, 516330, India
[2]Department of Mathematics, GITAM Deemed to be University, Hyderabad, 500081, India.
[3]Department of Mathematics, School of Computer Science and Artificial Intelligence, SR University, Warangal, 506371, India
[4]Department of Mathematics, St. Ann's College for Women, Hyderabad, 500028, India

ARTICLE INFO

Article history
Received: 14 November 2023
Revised: 17 January 2024
Accepted: 09 April 2024

Keywords:
Boundary Layer; Hybrid Nano Fluid; Magnetic Parameter; Maxwell Parameter; Prandtl Number; Stretching Sheet; UCM

ABSTRACT

The hybrid nanofluid (HNF) is widely used in manufacturing industrial applications because of its outstanding property of increasing the heat transfer process.The objective of this study was to measure the visco-elastic hybrid nanoliquid's flow patterns, heat, and mass transfer behaviors in the presence of a porous media and a magnetic field.Applicationsof this current study may be found in various Industries which include advanced cooling systems in electronics, enhanced lubrication in machinery, and improved heat transfer in aerospace engineering. Water is used as the host fluid when alumina-copper nanocomponents are used. Our system's leading PDEs are transformed into ODEs with the use of common similarity transformation. Subsequently, the ODEs were resolved using the RK-4 based shooting technique along with the Matlab program. The effects of pertinent parameters on fluid mass and heat transmission have then been discussed in support of the graphical and tabular approaches.The current study finds that with increased values of all the parameters, fluid velocity increases. It is predicted that with an increase in the elastic number of the Upper Convected Maxwell (UCM) hybrid fluid, the boundary layer will shrink and the wall skin friction coefficient will decrease.

Cite this article as: Thirupathi G, Govardhan K, Nagaraju G, Misra S. MHD upper-convected maxwell hybrid nano fluid over a stretching sheet: A numerical approach. Sigma J Eng Nat Sci 2025;43(2):429–440.

INTRODUCTION

The last several years have seen a significant amount of coverage from scientists and researchers about the development of enhanced heat transfer fluids. In industrial and technical applications, regular fluids including water, oil, and ethylene glycol are frequently utilized. However, because of their poor thermal conductivity, these fluids' capacity to transmit heat is constrained. Consequently, to remedy this shortcoming, a certain type of nanoparticles-referred to as "nanofluid"is added to the fluids. Nanofluids incorporate a small number of nanoparticles to enhance the thermal capacities of conventional fluids. In practice, the idea put out by Choi and Eastman [1] to incorporate nanoparticles

***Corresponding author.**
*E-mail address: nagaraju.gajjela@sru.edu.in

This paper was recommended for publication in revised form by Editor-in-Chief Ahmet Selim Dalkilic

into a base fluid has been successful. Some of the benefits of using nanofluids through a stretchable surface were studied by Kalidas [2] and Khanafer et al. [3]. Besides, the additional references on these topics can be found in the research papers [4-8].

The goal of developing hybrid nanofluid was to improve the standard nanofluid's thermal characteristics. Researchers typically choose hybrid nanofluids because they suspend two or more dissimilar nanoparticles in a typical heat transfer liquid, which are frequently utilized in numerous manufacturing, industrial, and biomedical engineering procedures. It seems that Suresh et al. [9] is the earliest researcher who considered the hybrid nano-composite particles in their experimental studies. Takabi and Shokouhmand [10] discovered that mixed Nanofluids not only improved the rate of thermal transfer but also reduced friction and pressure loss. Researchers Zainal et al. [11], Khashie et al. [12], Waini et al. [13], and Algehyne et al. [14] looked into Hybrid Nanofluids in their research. The mixed convection flow in a hybrid nanofluid across an exponentially stretching/shrinking vertical surface was studied by Waini et al. [15]. They discovered that when the nanoparticle volume fractions for copper increased, the rate of heat transfer decreased.

Many researchers in the fields of biomechanics, industry, and engineering have focused on extensive applications of Newtonian and non-Newtonian fluids in the boundary layer flow across a stretching surface. Magneto hydrodynamic (MHD) flow studies are important for various industries and find applications in metallurgical and petroleum-related processes. The first researcherto investigate the MHD flow of a non-Newtonian fluid was Sarpakaya [16]. Boundary layer theory has proven to be very useful in the case of Newtonian fluids, as it allows for the transformation of Navier-Stokes equations into more manageable boundary layer differential equations.Some application ofmodeling of differential equation can seen from [17-19]. Accordingly, Mahanta and Shaw[20], Ravichandra Nayakar et al. [21], Ahmed M. Megahed [22], Ram Prakash Sharma and Sachin Shaw[23], and Vishalakshi et al. [24] examined with different parameters on the non-Newtonian fluid flow past various stretching surfaces. Recently, numerous researchers explored the flow of different fluids with the impact of maragoni convection with magnetic effect and other influential factors [25–28].

One kind of viscoelastic or rate-type fluid is the upper-convected Maxwell fluid. Because it predicts the relaxation time impact and eliminates the complicated effects of shear-dependent viscosity, this model is highly significant. A common topic of study for numerous researchers is upper-convected Maxwell fluid flow. The effect of MHD flow and energy transmission on a stretched sheet was studied by Subhas et al. [29] using UCM fluid. It was shown that the velocity falls as the Maxwell parameter increases. Ishak et al. [30] have taken into consideration the problem of the MHD flow and heat transfer within a boundary layer of upper-convected Maxwell fluid over a stretching/shrinking sheet with prescribed heat flux. They infer that rising skin friction coefficient values are a direct result of rising magnetic parameter values. Non-Newtonian Maxwell fluids under various physical conditions, including porous media, transpiration, first-order chemical reactions, thermal radiation, heat source, and stretching surfaces, were examined by Amir and Kayva [31], Swati [32], Swati et al. [33], Vajravelu et al. [34], Gireesha et al. [35], and Ibrahim and Mekonnen [36]. Their findings demonstrate that temperature and heat transfer rate decreased as Prandtl number increased. Based on the research and an extensive literature review, it appears that there has been no previous investigation into the boundary layer flow and thermal transfer of UCM hybrid fluid over a stretched sheet. The aim of studying current research is to investigate the magnetohydrodynamics (MHD) behavior of upper-convected Maxwell hybrid nanofluids over a stretching sheet using numerical techniques. The scope includes analyzing fluid

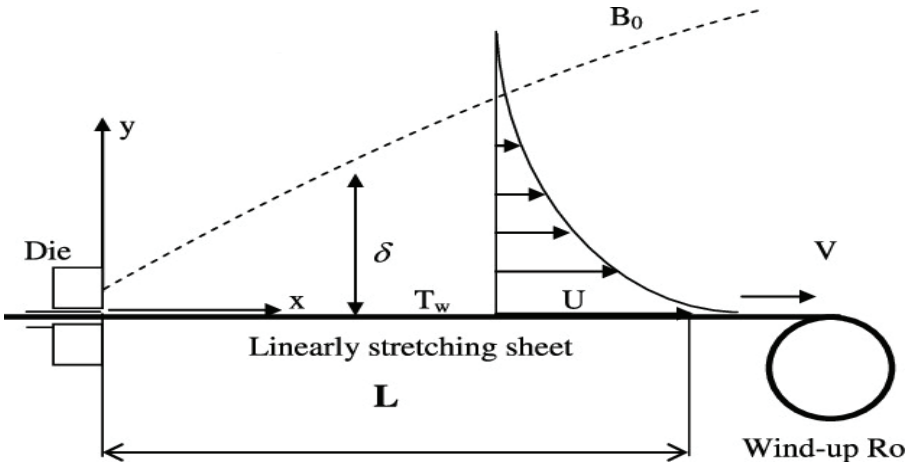

Figure 1. Diagram of the flow over a stretching sheet.

flow, heat transfer, and nanoparticle behavior under various parameters.

The data collected from the study will be analyzed using the bvp4c procedure in MATLAB to obtain the most optimal solution.

MATERIALS AND METHODS

Mathematical Formulation

We consider a laminar 2D boundary-layer flow and the Heat and mass transfer of an incompressible Maxwell Hybrid nano fluid (which are meant to have alumina and copper as two small ingredients and water as the host fluid) over stretching porous sheet.The flow is restricted to z =0 and the stretching velocity for a linear sheet is u_w = Bx.When a non-uniform magnetic field of starting intensity B_0 is applied in the direction normal to the surface (see in Fig. 1). Table 1 shows the thermo physical properties of base solutions and nanoparticles. Under these conditions, our system's main equations are as follows:

Continuity equation:

$$\frac{\partial u}{\partial x}+\frac{\partial v}{\partial y}=0 \tag{1}$$

Momentum equation:

$$u\frac{\partial u}{\partial x}+v\frac{\partial v}{\partial y}+\lambda\left(u^2\frac{\partial^2 u}{\partial x^2}+v^2\frac{\partial^2 u}{\partial y^2}+2uv\frac{\partial^2 u}{\partial x\partial y}\right) = \frac{\mu_{hnf}}{\rho_{hnf}}\frac{\partial^2 u}{\partial y^2}-\frac{\mu_{hnf}}{\rho_{hnf}k_0}u-\frac{\sigma_{hnf}B_0^2}{\rho_{hnf}}u \tag{2}$$

Energy equation:

$$u\frac{\partial T}{\partial x}+v\frac{\partial T}{\partial y}=\kappa_{hnf}\left(\frac{\partial^2 T}{\partial x^2}+\frac{\partial^2 T}{\partial y^2}\right)+\frac{(\rho C_p)_f}{(\rho C_p)_{hnf}}D_B\left(\frac{\partial C}{\partial x}\frac{\partial T}{\partial x}+\frac{\partial C}{\partial y}\frac{\partial T}{\partial y}\right) + \left(\frac{D_T}{T_\infty}\right)\left[\left(\frac{\partial T}{\partial x}\right)^2+\left(\frac{\partial T}{\partial y}\right)^2\right] \tag{3}$$

Concentration Equation:

$$u\frac{\partial C}{\partial x}+v\frac{\partial C}{\partial y}=D_B\left(\frac{\partial^2 C}{\partial x^2}+\frac{\partial^2 C}{\partial y^2}\right)+\left(\frac{D_T}{T_\infty}\right)\left(\frac{\partial^2 T}{\partial x^2}+\frac{\partial^2 T}{\partial y^2}\right) \tag{4}$$

In this, x and y are the directions that are parallel and perpendicular to the sheet. The velocity components u and v are taken along the x and y directions. T stands for Maxwell hnf' s temperature, ρ_{hnf} designates Maxwell Hybrid Nanofluid's density, σ_{hnf} indicates for electrical conductivity of hybrid nano suspension, κ_{hnf} stands for Maxwell Hybrid Nanofluids heat/thermal conductivity, $(\rho c_P)_{\text{hnf}}$ is the Maxwell Hybrid Nanofluid's specific heat, B0stands magnetic field's amplitude, B >0 indicates the rate at which it is stretching, λ is the Maxwell parameter, μ is the fluid's kinematic viscosity.

Boundary conditions:

The appropriate flow boundary conditions are

$$u=Bx,\ v=0, T=T_w,\ C=C_w \text{ at } y=0,\quad u=0,\ T\to T_\infty, \text{C}\to C_\infty \text{ at } y\to\infty \tag{5}$$

The subscripts *hnf, f* stand for "hybrid nano liquid," "base fluid", 1 and 2 stand for "Cu" and "Al_2O_3 nanoparticles," and ϕ_1, ϕ_2 stand for "volume fraction", respectively.

Table 1. Thermo-physical properties of the nano particles and water (Suresh et al.[9])

Physical properties	Cu	Water	Al_2O_3
C_p/JKg^{-1} K	385	4180	765
ρ/Kgm^{-3}	8933	997	3970
κ/WmK^{-1}	400	0.6071	40

Table 2. The correlations of single(NF) and hybrid nano fluids (HNF) (Takabi et al [10], Zainal et al [11])

Properties	Hybrid Nanofluids Al_2O_3–Cu/water
Density	$\rho_{hnf}=(1-\phi_1-\phi_2)\rho_f+\phi_1\rho_1+\phi_2\rho_2$
Thermal capacity	$(\rho C_p)_{hnf}=(1-\phi_1-\phi_2)(\rho C_p)_f+\phi_1(\rho C_p)_1+\phi_2(\rho C_p)_2$
Dynamic viscosity	$\mu_{hnf}=\frac{\mu_f}{(1-\phi_1-\phi_2)^{2.5}}$
Thermal conductivity	$\frac{k_{hnf}}{k_f}=\left\{\frac{\phi_1k_1+\phi_2k_2}{\phi_1+\phi_2}+2k_f+2(\phi_1k_1+\phi_2k_2)-2(\phi_1+\phi_2)k_f\right\}\times\left\{\frac{\phi_1k_1+\phi_2k_2}{\phi_1+\phi_2}+2k_f-2(\phi_1k_1+\phi_2k_2)+(\phi_1+\phi_2)k_f\right\}^{-1}$

Similarity transformation:

We have chosen the following similarity functions to transform the first (1-4) equations into their dimensionless form:

$$u = Bxf'(\eta),\ v = -\sqrt{vB}\, f(\eta),\ \eta = \left(\frac{B}{v}\right)^{\frac{1}{2}} y,$$
$$\theta(\eta) = \frac{T-T_\infty}{T_w-T_\infty},\ \phi(\eta) = \frac{C-C_\infty}{C_w-C_\infty} \quad (6)$$

Equations (1-4) yield the following results using the similarity approach described above:

$$\frac{A_1}{A_2} f''' - \frac{M^2}{A_2} f' - (f')^2 + ff'' + \beta[2ff'f'' - f^2 f'''] - \frac{k_p}{A_2} f' = 0 \quad (7)$$

$$A_3\theta'' + \frac{P_r}{A_4}[f\theta' + N_b\theta'\phi' + N_t(\theta')^2] = 0 \quad (8)$$

$$\phi'' + L_e P_r f\theta' + \frac{N_t}{N_b}\theta'' = 0 \quad (9)$$

Here, the prime indicates the derivative with respect to η and

$$A_1 = \frac{\mu_{hnf}}{\mu_f},\ A_2 = \frac{\rho_{hnf}}{\rho_f},\ A_3 = \frac{\kappa_{hnf}}{\kappa_f},\ A_4 = \frac{(\rho C_p)_{hnf}}{(\rho C_p)_f},$$

Subsequently the boundary conditions are taken in the form,

$$f(0)=0,\ f'(0)=1,\ f'(\infty)=0,\ \theta(0)=1,\ \theta(\infty)=0,$$
$$\phi(0)=1,\ \phi(\infty)=0 \quad (10)$$

Here $M^2 = \frac{\sigma B_0^2}{\rho_f B}, \beta = \lambda B, k_p = \frac{\mu_f}{\rho_f \kappa_0 B}, P_r = \frac{\nu_f}{\alpha_f}, Le = \frac{\alpha}{D_B}$, $N_t = \frac{D_T(T_w-T_\infty)}{\nu T_\infty (\rho C_p)_f}, N_b = \frac{D_B(C_w-C_\infty)}{\nu(\rho C_p)_f}$

The Nusselt number, a conventional dimensionless expression of the rate of heat transmission between a surface and a fluid,is given by

$$Nu_x = -\frac{x\kappa_{hnf}}{\kappa_f(T_w-T_\infty)}\left(\frac{\partial T}{\partial y}\right)_{y=0} = -\frac{\kappa_{hnf}}{\kappa_f}\sqrt{Re_x}\,\theta'(0),$$
$$\text{We have } Nu_x(Re_x)^{-\frac{1}{2}} = -\frac{\kappa_{hnf}}{\kappa_f}\theta'(0) \quad (11)$$

Skin friction coefficient and Sherwood number are given by

$$Cf_x = -\frac{\mu_{hnf}}{\rho_f u_w^2}\left(\frac{\partial u}{\partial y}\right)_{y=0}, \text{ we have } Cf_x(Re_x)^{\frac{1}{2}} = \frac{\mu_{hnf}}{\mu_f} f''(0) \quad (12)$$

$$\text{And } Sh_x(Re_x)^{-\frac{1}{2}} = -\phi'(0) \quad (13)$$

Where Re_x, Nu_x, and Sh_x are, respectively, local Reynolds, Nusselt, and Sherwood numbers.

NUMERICAL SOLUTION AND METHODOLOGY

It is worth mentioning that the Prandtl number was fixed at 6.2 (representing water) throughout the analysis of this study (zainal et al [11]). Obeying the remarkable work of Suresh et al. [9], the nanoparticles' volume concentration of this study was set within the range of 0.005 0.015 to ensure the stability of the hybrid nanofluid. Meanwhile, the other parameters were used between these ranges (excluding the validation part): $0 < M^2 < 2$ (magnetic parameter), $0 < \beta, k_p < 1$ (Maxwell and porosity parameter) and $0 < Le, Nt, Nb < 1.5$. Further, the bvp4c in Matlab was fully utilized to solve the ordinary and reduced differential equation systems of Equations (7) and (9) together with the boundary equations (see Equation (10)).

Thus, utilizing the RK-4-based shooting technique, the necessary velocity profiles, temperature fields, and concentration profiles with boundary conditions (10) have been drawn. First, the primary equations governing the flow are transformed into 1st order ODEs, and then an RK-4 procedure with shooting criteria is used to execute stepwise integration. All of the solution profiles have been generated using MATLAB.

The Program and Algorithm

The analytic solution of the boundary value problem Eqns. (7)-(9) cannot be found because these equations are non-linear and coupled. The system of nonlinear ODEs Eqns. (7)-(9) along with boundary condition Eqn. (10) are converted into first order ODEs. The first order systems of ODEs with appropriate boundary condition are solved by using shooting method. We adopt the following procedure:

$$f''' = \frac{1}{\left(\frac{A_1}{A_2} - \beta f^2\right)}\left[\frac{M^2}{A_2} f' + (f')^2 - ff'' - 2\beta ff'f'' + \frac{k_p}{A_2} f'\right] \quad (14)$$

$$\theta'' = -\frac{P_r}{A_3 A_4}[f\theta' + N_b\theta'\phi' + N_t(\theta')^2] \quad (15)$$

$$\phi'' = -L_e P_r f\theta' - \frac{N_t}{N_b}\theta'' \quad (16)$$

Since Eq. (14) is a function of f and its derivatives, which can be solved numerically by shooting method. The solution of Eq. (14) can be used in Eq. (15) and Eq. (16) as a known input.

For further proceeding, use the following notations:

$$f = y_1, \quad \theta = y_4, \quad \phi = y_6. \quad (17)$$

The coupled nonlinear flow equations are turned into the subsequent system of seven first order ODEs together with the initial conditions:

$$
\begin{aligned}
y_1' &= y_2, & y_1(0) &= 0,\\
y_2' &= y_3, & y_2(0) &= 1,\\
y_3' &= \frac{1}{\left(\frac{A_1}{A_2}-\beta f^2\right)}\left[\frac{M^2}{A_2}\, y_2 + (y_2)^2 - y_1\, y_3 - 2\beta\, y_1\, y_2\, y_3 + \frac{k_p}{A_2}\, y_2\right], & y_3(0) &= \mathrm{p},\\
y_4' &= y_5, & y_4(0) &= 0,\\
y_5' &= -\frac{P_r}{A_3 A_4}[f y_5 + N_b y_5 y_7 + N_t (y_5)^2], & y_5(0) &= t,\\
y_6' &= y_7, & y_6(0) &= 1,\\
y_7' &= -L_e P_r\, y_1\, y_5 - \frac{N_t}{N_b}\, y_6, & y_7(0) &= u.
\end{aligned}
$$

The RK method has been taken into consideration for solving the above initial value problem. In the above system of equations, the missing conditions are to be chosen such that

$$
\left(y_3(\eta_\infty, p, t, u)\right)_{\eta=\eta_\infty} = 0, \left(y_5(\eta_\infty, p, t, u)\right)_{\eta=\eta_\infty} = 0,
$$

$$
\left(y_7(\eta_\infty, p, t, u)\right)_{\eta=\eta_\infty} = 0.
$$

RESULTS AND DISCUSSION

This part describes how the parameters affect the flow features. The required parameters effectson velocity, concentration, and temperature have been explored and described.

Figures 2, 3, and 4 show how the magnetic field parameter affects flow velocity, temperature, and concentration. The figures indicate that the fluid's velocity dropped as the magnetic field increased, whereas the temperature and concentration profiles showed a rising pattern.This is because the magnetic field acts as a retarding body force, or Lorentz

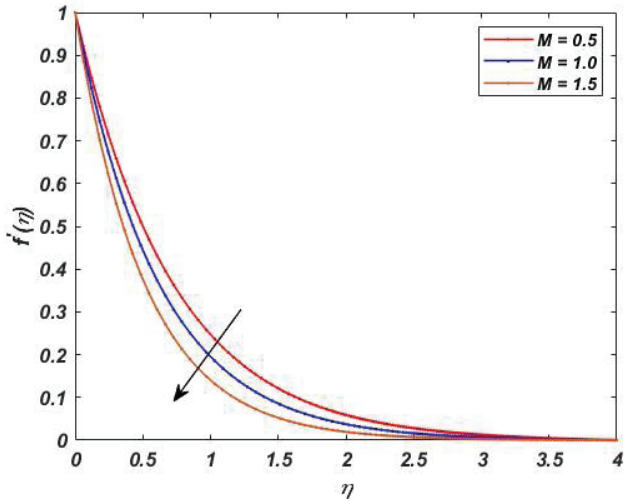

Figure 2. Effect of magnetic field M on $f'(\eta)$.

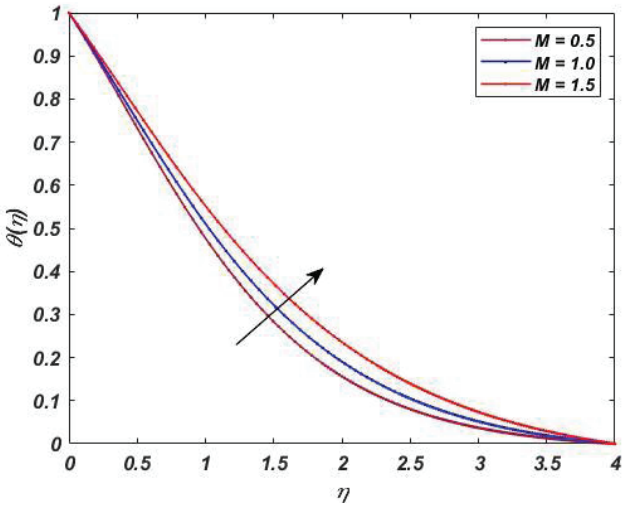

Figure 3. Impact of Mon $\theta(\eta)$.

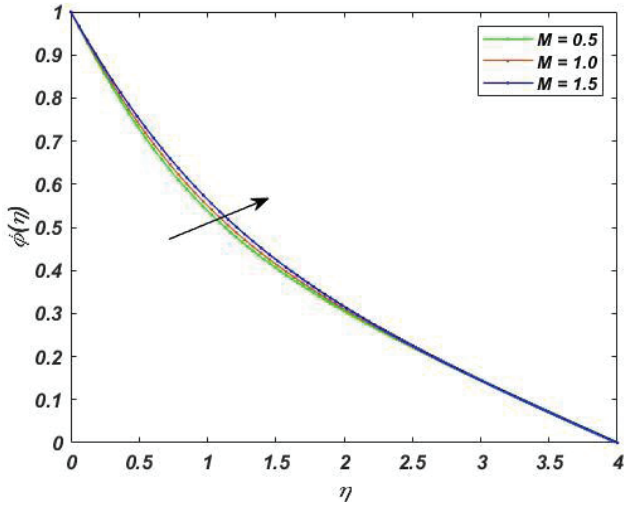

Figure 4. Impact of M on $\phi(\eta)$.

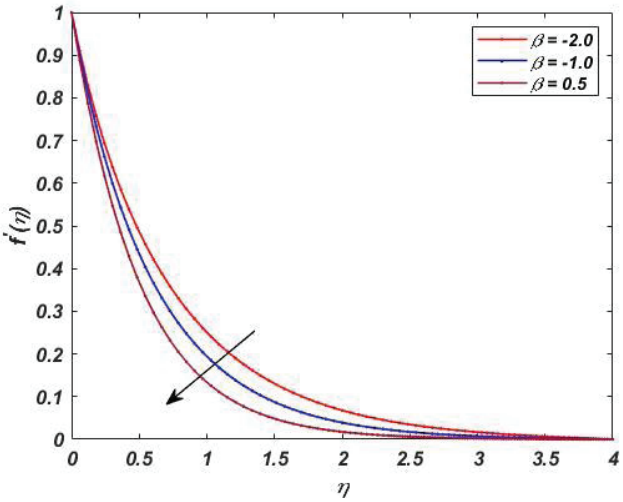

Figure 5. Impact of β on $f'(\eta)$.

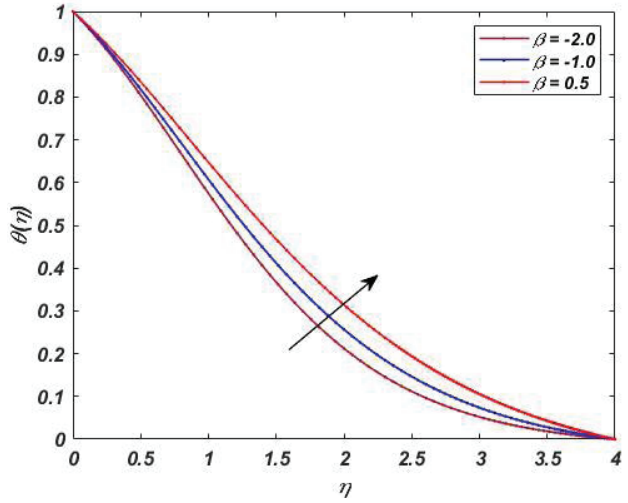

Figure 6. Impact of β on $\theta(\eta)$.

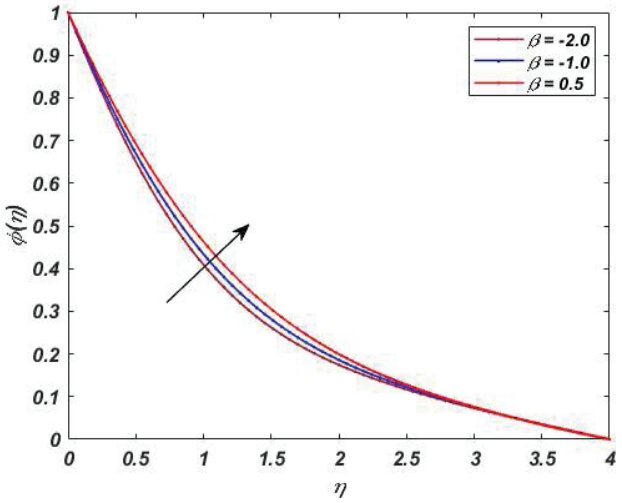

Figure 7. Impact of β on $\phi(\eta)$.

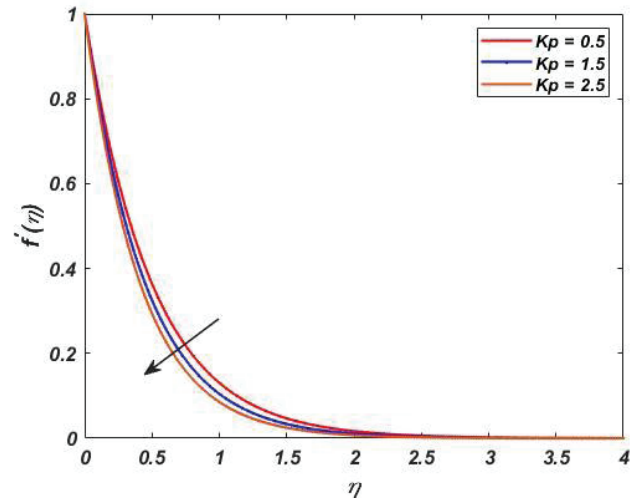

Figure 8. Impact of k_p on $f'(\eta)$.

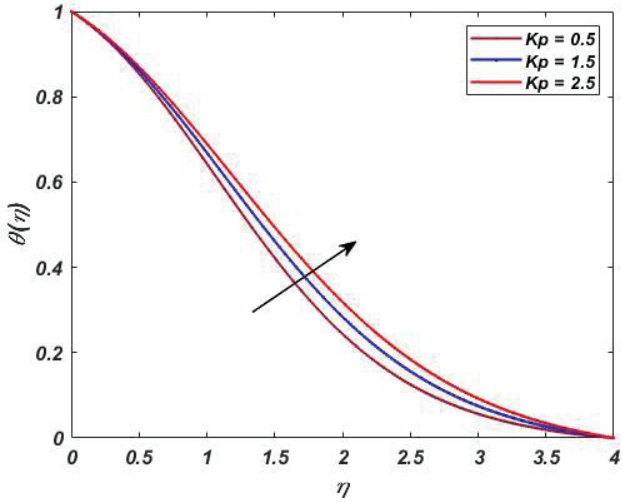

Figure 9. Impact of k_p on $\theta(\eta)$.

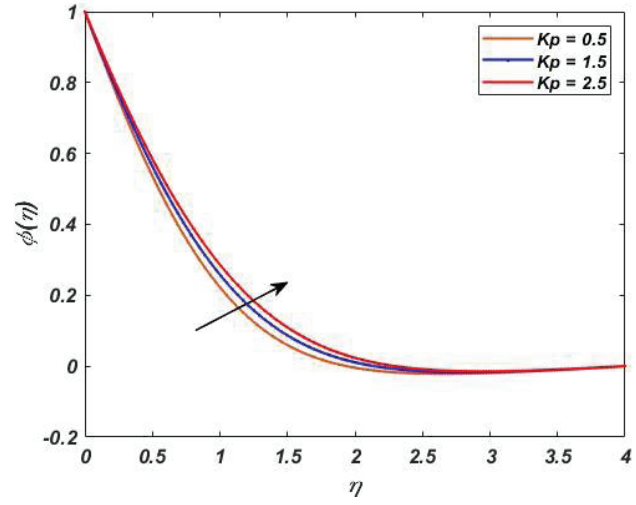

Figure 10. Impact of k_p on $\phi(\eta)$.

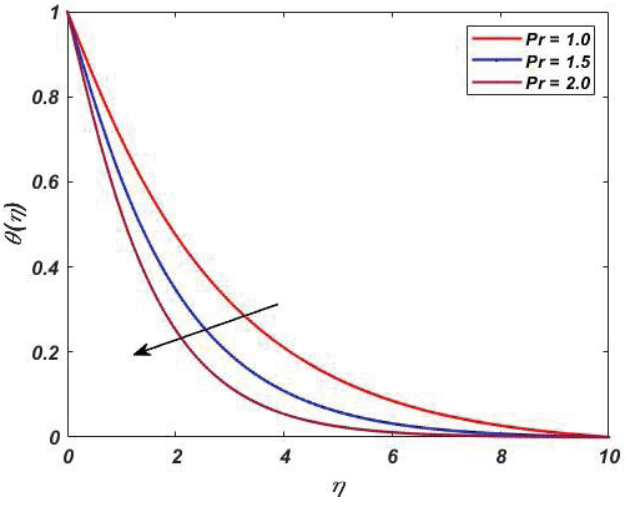

Figure 11. Impact of P_r on $\theta(\eta)$.

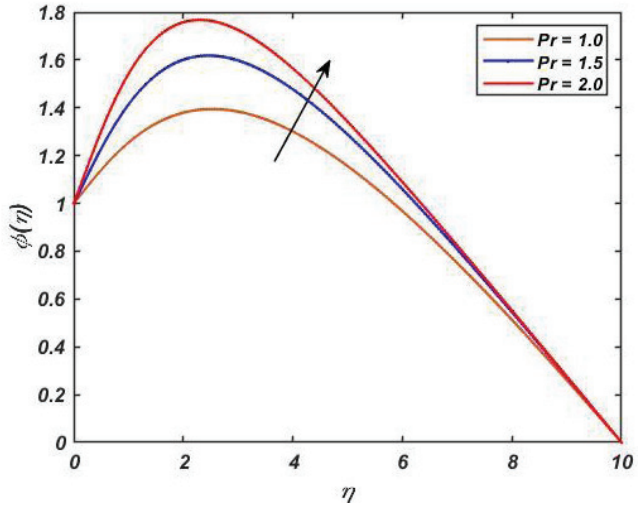

Figure 12. Impact of P_r on $\phi(\eta)$.

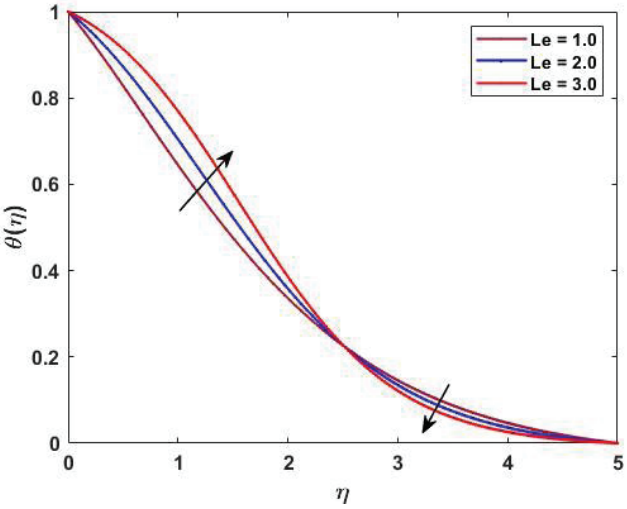

Figure 13. Impact of Le on $\theta(\eta)$.

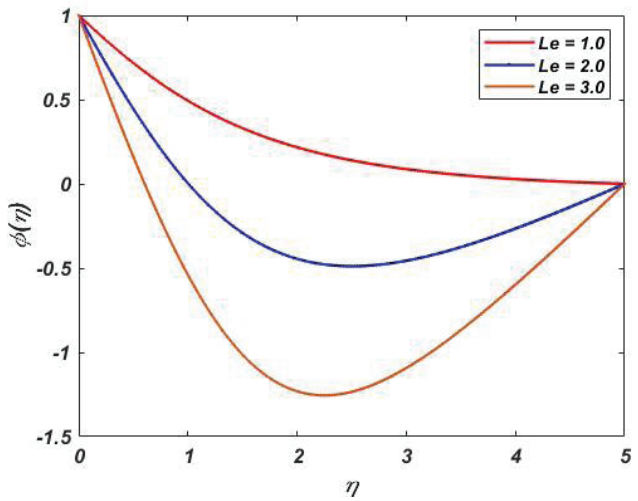

Figure 14. Impact of Le on $\phi(\eta)$.

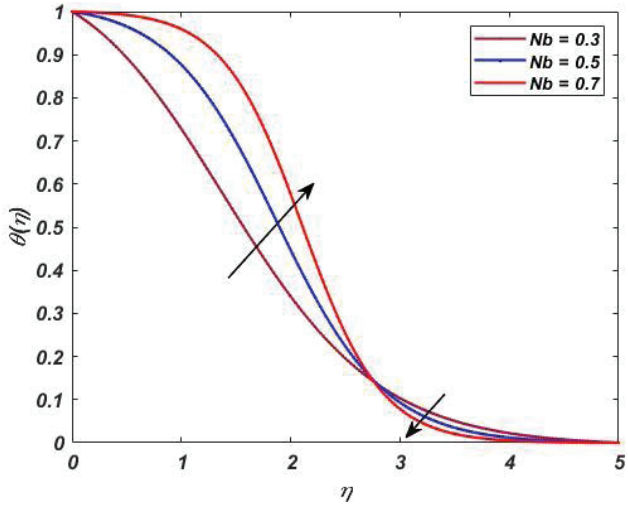

Figure 15. Impact of N_b on $\theta(\eta)$.

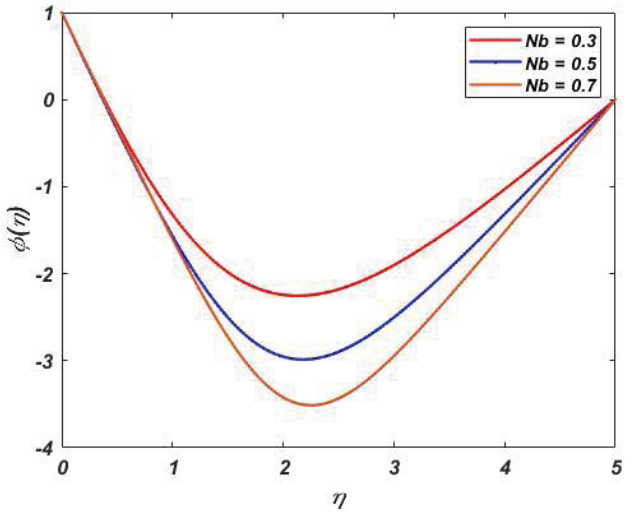

Figure 16. Impact of N_b on $\phi(\eta)$.

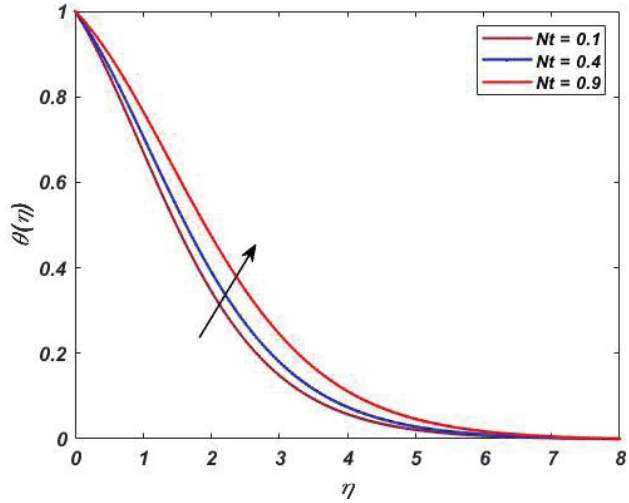

Figure 17. Impact of N_t on $\theta(\eta)$.

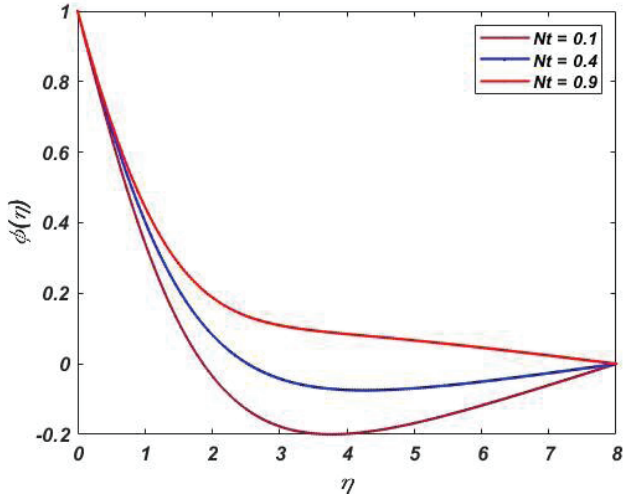

Figure 18. $\phi(\eta)$ for distinct values of N_t.

force, acting in a direction perpendicular to the direction of the applied magnetic field. This body force restricts both the momentum boundary layer's thickness and the boundary layer's flow. Similarly, heat is produced by the Lorentz force, a fractional resistive force that resists fluid motion. This means that the concentration and thermal boundary layers are thicker under stronger magnetic fields.Figures 5, 6, and 7 depict the influences of the Maxwell constant on the profiles of velocity, concentration, and temperature over the sheet. An increase in the Maxwell parameter tumbles fluid velocity while increasing the fluid's temperature and concentration Profiles. When the Maxwell parameter increases, it suggests that the viscous-elastic effects in the fluid become more pronounced. These effects can manifest as a boost in fluid's elastic properties, resulting in a reduction in the fluid's ability to flow easily. This increased resistance to flow causes the fluid velocity above the sheet to decrease. The association between the Maxwell parameter and thermal boundary layer thickening is presumably mediated by the interaction between these non-Newtonian properties and the heat transfer process. As the Maxwell parameter increases, it likely influences the fluid's viscosity or flow behavior, causing changes in the properties of heat transfer. These changes can lead to a thicker thermal boundary layer.The effects of the porosity measure on the temperature, concentration, and velocity profiles are shown in Figures 8, 9, and 10. It has been noted that when the porosity parameter value grows, the concentration and temperature rise and the velocity gradient decreases. As Kp increases, it implies that the porous medium becomes more resistant to fluid flow. However, in porous media, increased resistance to fluid flow (as indicated by higher) can result in greater heat transfer between the fluid and the porous medium. This enhanced heat transfer can lead to higher temperatures in the fluid, causing the temperature graph to increase. Like the temperature effect, the increased resistance to fluid flow in the porous medium (higher) can influence mass transport processes. This can lead to enhanced concentration gradients and increased concentration in the fluid as it passes through the porous medium.

Figures 11 and 12 depict how the graphs of temperature and concentration change in relation to the Prandtl number, respectively. As shown in Figure 11, when the Prandtl number goes up, the temperature and the thickness of the thermal boundary go down. This is because a fluid with a high Pr value has a relatively low thermal conductivity, which reduces conduction and, as a result, diminishes the width of the thermal boundary layer. As evidenced in Figure 12, the thickness of the concentration boundary layer increases as Pr values rise. Figures 13 and 14 depict temperature and concentration graphs with respect to the Lewis number (Le). The temperature profile increased for high Le values. The concentration profile decreased for high Le values, resulting in a small molecular diffusivity. Typically, as the Lewis number rises, the concentration profile falls. Furthermore, as the Lewis number rises, the concentration boundary layer becomes thinner. Most likely, this is because the mass transfer rate goes up as the Lewis number goes up. The concentration gradient within the sheet is also increased. Temperature and concentration graphs vary with Brownian motion parameter in Figures 15 and 16, respectively. As Nb values rise, the temperature graph rises. Physically, Nb is associated with fluid particle movement. The kinetic energy of the particles in a fluid rises as rises. The thermal boundary layer thickens as increases, as shown in the graph. Figure 16 indicates that concentration distribution decreases as Nb increases. Thermophoresis parameter Nt affects temperature and concentration profiles, as shown in Figures 17 and 18. As depicted in graph 17, the fluid's temperature profile rises as Nt values increase. In the presence of Nt, the nanoparticles on the hot boundary side have been shifted to the cold boundary side, and the thermal boundary layer has thickened. As shown in Figure 18, the thickness of the concentration boundary layer increases as Nt rises. Increasing is observed to increase the concentration distribution progressively.

Nusselt Number, Sherwood Number, and Skin Friction Coefficient

Tables 1 and 2 describe the computed numerical results of the Skin friction coefficient, Nusselt number, and Sherwood number using various physical parameters listed in the tables.

The skin friction coefficient quantifies the quantity of friction encountered by a fluid as it flows along a solid boundary. A greater value for the skin friction coefficient indicates increased fluid flow resistance.

The coefficient of skin friction is displayed against applied magnetic field strength M is portrayed in figure 19. As β values increase, $-f''(0)$ rises. This implies that with increasing β, the skin friction experienced by the fluid near the boundary increases. This behavior suggests that the

Table 1. Numerical values of $-f''(0)$ for Kp = 0.4; Le = 1; Pr = 2; Nt = 0.5; Nb = 0.5.

β	M	$-f''(0)$
0.1	0.5	1.314333
	1.0	1.562026
	1.5	1.904705
0.5	0.5	1.396169
	1.0	1.630561
	1.5	1.960667
0.9	0.5	1.458525
	1.0	1.697258
	1.5	2.015690

Table 2. Numerical values of $-f''(0)$,$-\theta'(0)$ and $-\phi'(0)$ for $\beta = 2$, Pr = 2, $K_p = 3$, Le = 2, M = 1.5.

N_b	N_t	$-\theta'(0)$	$-\phi'(0)$
0.3	0.1	0.295334	1.002193
	0.4	0.253242	0.874197
	0.9	0.190129	0.815933
0.5	0.1	0.173982	1.052268
	0.4	0.144364	1.027266
	0.9	0.102731	1.040295
0.7	0.1	0.088687	1.057716
	0.4	0.071113	1.058810
	0.9	0.048080	1.077868

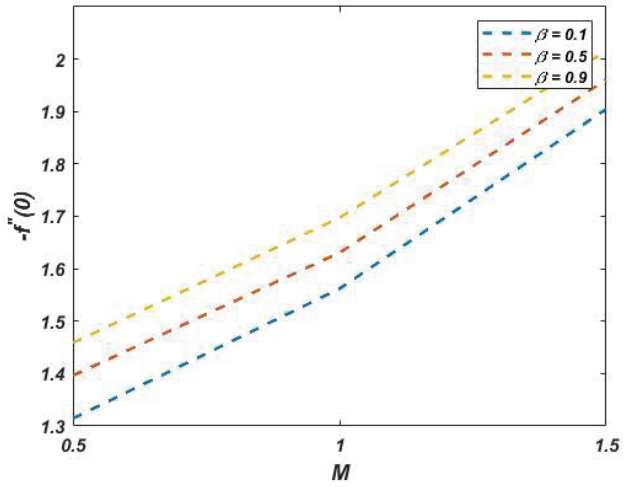

Figure 19. Graph of $-f''(0)$ for distinct values of M.

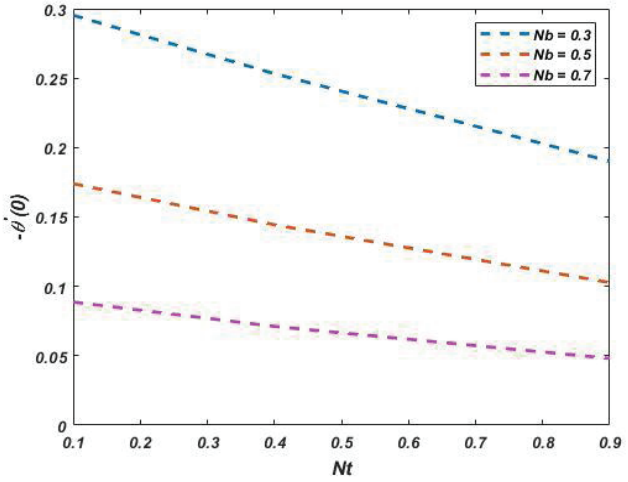

Figure 20. Graph of $-\theta'(0)$ for distinct values of Nt.

flow is more impeded; leading to a greater resistance to flow and skin friction coefficient.Figure 20 illustrates the influence of the Brownian motion variable on the Nusselt number in comparison to the thermophoresis parameter. This suggests that increasing the Brownian motion parameter decreases heat transfer at the specific location. The influence of Brownian motion on the Nusselt number could be due to enhanced particle dispersion or reduced convective heat transfer, which can hinder heat transfer at the surface. Figure 21 illustrates how the thermophoresis parameter influences the local Sherwood number $-\phi'(0)$ in relation to the Brownian motion parameter. As N_t values increase, the local Sherwood number graph also increases. The thermophoresis parameter relates to the thermophoresis phenomenon, which is the motion of particles induced by temperature gradients. The impact of increasing the thermophoresis parameter on Sherwood number could be due

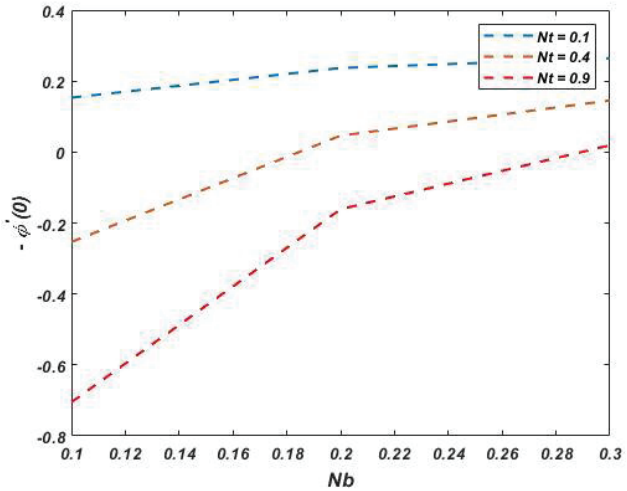

Figure 21. Graphof $-\phi'(0)$ for distinct values of Nb.

to enhanced particle concentration or improved diffusion of species near the surface. The enhanced thermophoresis parameter influences species transport near the surface, thickening the concentration boundary layer.

CONCLUSION

A numerical investigation of the boundary layer and MHD flow of UCM hybrid Nano fluidsover a stretching sheetwas provided.This work will undoubtedly be useful for many applications in (i) Heat transfer enhancement in industrial processes, (ii) Optimization of cooling systems in electronic devices, (iii) Designing efficient lubricants for high-speed machinery, (iv) Understanding fluid dynamics in biomedical applications, like drug delivery systems and (v) Improving the performance of aerospace propulsion systems.

The primary equations governing the flow were converted into a set of ODEs using similarity variables, and numerical solutions for various governing parameters were provided. The mathematical model is solved using bvp5c technique. The substantial consequences of numerous physical factors on non-dimensional profiles of velocity, temperature, concentration, coefficient of skin friction, local Nusselt number, and local Sherwood number are graphically shown.

The study yields the following conclusions:

- When the Maxwell parameter values are increased, the velocity boundary layer thickness is observed to decrease.
- As thehigh intensity of magnetic field is applied, the magnetic field boundary layer becomes thinner.
- Increasing Maxwell parameter causes the high molecular velocity, which enhances temperature field, concentration profile, and boundary layer thickness.
- The thickness of the concentration boundary layer decreases as the Lewis number Le and Brownian motion N_b increase, while it increases as N_t values rise.
- The surface temperature increases for increasing values of porous parameter K_p, N_b and N_t, but it decreases as Pr values were increased during observations.
- The present investigations are useful in industrial application as well as in the botanical segment limited to their experimental existence.

Future Scope: We can analyse this work using advanced computational techniques such as machine learning algorithms for getting more accurate predictions of fluid behaviour. Additionally, investigating the application of this fluid model in industrial processes like nanotechnology manufacturing or biomedical engineering could open new avenues for technological innovation and development.

AUTHORSHIP CONTRIBUTIONS

G. Thirupathi executed the numerical code and drawn all the graphs and tables; K. Govardhan did mathematical modelling of the problem andwrote the concerned parts of the manuscript and formatted it to the journal specification; G. Nagaraju wrote introduction part and performed drafting in the manuscript; Santoshi Misrarevised the manuscript and added themissing contents.

DATA AVAILABILITY STATEMENT

The authors confirm that the data that supports the findings of this study are available within the article. Raw data that support the finding of this study are available from the corresponding author, upon reasonable request.

CONFLICT OF INTEREST

The author declared no potential conflicts of interest with respect to the research, authorship, and/or publication of this article.

ETHICS

There are no ethical issues with the publication of this manuscript.

REFERENCES

[1] Choi SUS. Enhancing thermal conductivity of fluid with nanoparticles. ASME Fluids Eng Div 1995;231:99–105. [CrossRef]

[2] Das K. Nanofluid flow over a non-linear permeable stretching sheet with partial slip. J Egypt Math Soc 2015;23:451–456. [CrossRef]

[3] Khanafer K, Vafai K, Lightstone M. Buoyancy-driven heat transfer enhancement in a two-dimensional enclosure utilizing nanofluids. Int J Heat Mass Transf 2003;46:3639–3653. [CrossRef]

[4] Jauhri S, Mishra U. Numerical investigation of MHD nanofluid considering second-order velocity slip effect over a stretching sheet in porous media. J Integr Sci Technol 2023;11:478.

[5] Gajjela N, Garvandha M. Impacts of variable thermal conductivity and mixed convective stagnation-point flow in a couple stress nanofluid with viscous heating and heat source. Heat Transfer 2020;49:3630–3650. [CrossRef]

[6] Matta A, Nagaraju G. The influence of double diffusive gradient boundary condition on micropolar nanofluid flow through a stretching surface with a higher-order chemical reaction. Int J Comput Sci Math 2021;14:301–313. [CrossRef]

[7] Khan MN, Nadeem S. A comparative study between linear and exponential stretching sheet with double stratification of a rotating Maxwell nanofluid flow. Surf Interfaces 2021;22:100886. [CrossRef]

[8] Rama Devi SVV, Gnaneswara Reddy M. Parametric analysis of MHD flow of nanofluid in stretching sheet under chemical sensitivity and thermal radiation. Heat Transfer 2022;51:948–975. [CrossRef]

[9] Suresh S, Venkitaraj KP, Selvakumar P, Chandrasekar M. Effect of Al_2O_3–Cu/water hybrid nanofluid in heat transfer. Exp Therm Fluid Sci 2012;38:54–60. [CrossRef]
[10] Takabi B, Shokouhmand H. Effects of Al_2O_3–Cu/water hybrid nanofluid on heat transfer and flow characteristics in turbulent regime. Int J Mod Phys C 2015;26:1550047. [CrossRef]
[11] Zainal NA, Nazar R, Naganthran K, Pop I. Impact of anisotropic slip on the stagnation-point flow past a stretching/shrinking surface of the Al_2O_3–Cu/H_2O hybrid nanofluid. Appl Math Mech 2020;41:1401–1416. [CrossRef]
[12] Khashi'ie NS, Waini I, Zokri SM, Kasim ARM, Arifin NM, Pop I. Stagnation point flow of a second-grade hybrid nanofluid induced by a Riga plate. Int J Numer Methods Heat Fluid Flow 2021;32:2221–2239. [CrossRef]
[13] Waini I, Ishak A, Pop I. Flow towards a stagnation region of a curved surface in a hybrid nanofluid with buoyancy effects. Mathematics 2021;9:2330. [CrossRef]
[14] Algehyne EA, El-Zahar ER, Elhag SH, Bayones FS, Nazir U, Sohail M, et al. Investigation of thermal performance of Maxwell hybrid nanofluid boundary value problem in vertical porous surface via finite element approach. Sci Rep 2022;12:2335. [CrossRef]
[15] Waini I, Ishak A, Pop I. Mixed convection flow over an exponentially stretching/shrinking vertical surface in a hybrid nanofluid. Alex Eng J 2020;59:1881–1891. [CrossRef]
[16] Sarpkaya T. Flow of non-Newtonian fluids in a magnetic field. AIChE J 1961;7:324–328. [CrossRef]
[17] Dubey R, Mishra LN, Sanchez Ruiz LM, Sarwe DU. Nondifferentiable multiobjective programming problem under strongly K-Gf-pseudoinvexity assumptions. Mathematics 2020;8:738. [CrossRef]
[18] Sharma N, Mishra LN, Mishra VN, Pandey S. Solution of delay differential equation via N^v_1 iteration algorithm. Eur J Pure Appl Math 2020;13:1110–1130. [CrossRef]
[19] Dubey R, Kumar R, Alam K, Narayan ML, Narayan MV. A class of new type unified non-differentiable higher order symmetric duality theorems over arbitrary cones under generalized assumptions. YUJOR 2022;32:189–202. [CrossRef]
[20] Mahanta G, Shaw S. 3D Casson fluid flow past a porous linearly stretching sheet with convective boundary condition. Alex Eng J 2015;54:653–659. [CrossRef]
[21] Nayakar R, Mahabaleshwar US, Vinaykumar PN, Lorenzini G, Baleanu D. Nonlinear stretching/shrinking cooling of a sheet involving an MHD Walters' liquid B with suction. Math Model Eng Probl 2019;6:343–348. [CrossRef]
[22] Megahed AM. Williamson fluid flow due to a non-linearly stretching sheet with viscous dissipation and thermal radiation. J Egypt Math Soc 2019;27:12. [CrossRef]
[23] Sharma RP, Shaw S. MHD Non-Newtonian fluid flow past a stretching sheet under the influence of non-linear radiation and viscous dissipation. J Appl Comput Mech 2022;8:949–961.
[24] Vishalakshi AB, Mahabaleshwar US, Sarris IE. An MHD fluid flow over a porous stretching/shrinking sheet with slips and mass transpiration. Micromachines 2022;13:116. [CrossRef]
[25] Manjunatha N, Sumithra R. Non-Darcian-Bènard double diffusive magneto-Marangoni convection in a two-layer system with constant heat source/sink. Iraqi J Sci 2021;4039–4055. [CrossRef]
[26] Manjunatha N, Sumithra R. Effects of heat source/sink on Darcian-Benard-Magneto-Marangoni convective instability in a composite layer subjected to nonuniform temperature gradients. TWMS J Appl Eng Math 2022;12:969–984.
[27] Balaji VK, Narayanappa M, Udhayakumar R, AlNemer G, Ramakrishna S, Honnappa GY. Effects of LTNE on two-component convective instability in a composite system with thermal gradient and heat source. Mathematics 2023;11:4282. [CrossRef]
[28] Yellamma, Manjunatha N, Abdulrahman A, Khan U, Sumithra R, Gill HS, et al. Triple diffusive Marangoni convection in a fluid-porous structure: Effects of a vertical magnetic field and temperature profiles. Case Stud Therm Eng 2023;43:102765. [CrossRef]
[29] Subhas Abel M, Tawade JV, Nandeppanavar MM. MHD flow and heat transfer for the upper-convected Maxwell fluid over a stretching sheet. Meccanica 2012;47:385–393. [CrossRef]
[30] Ishak N, Hashim H, Mohamed MKA, Sarif NM, Khaled M, Rosli N, et al. MHD flow and heat transfer for the upper-convected Maxwell fluid over a stretching/shrinking sheet with prescribed heat flux. AIP Conf Proc 2015;1691:040011. [CrossRef]
[31] Alizadeh-Pahlavan A, Sadeghy K. On the use of homotopy analysis method for solving unsteady MHD flow of Maxwellian fluids above impulsively stretching sheets. Commun Nonlinear Sci Numer Simul 2009;14:1355–1365. [CrossRef]
[32] Mukhopadhyay S. Upper-convected Maxwell fluid flow over an unsteady stretching surface embedded in porous medium subjected to suction/blowing. Z Naturforsch A 2012;67:641–646. [CrossRef]
[33] Mukhopadhyaya S, Arif MG, Ali MW. Effects of transpiration on unsteady MHD flow of an upper convected Maxwell (UCM) fluid passing through a stretching surface in the presence of a first order chemical reaction. Chin Phys B 2013;22:124701. [CrossRef]
[34] Vajravelu K, Li R, Dewasurendra M, Benarroch J, Ossi N, Zhang Y, et al. Analysis of MHD boundary layer flow of an Upper-Convected Maxwell fluid with homogeneous-heterogeneous chemical reactions. Commun Numer Anal 2017;2:202–216. [CrossRef]

[35] Gireesha BJ, Mahanthesh B, Gorla RSR, Krupalakshmi KL. Mixed convection two-phase flow of Maxwell fluid under the influence of non-linear thermal radiation, non-uniform heat source/sink and fluid-particle suspension. Ain Shams Eng J 2018;9:735–746. [CrossRef]

[36] Ibrahim W, Negera M. MHD slip flow of upper-convected Maxwell nanofluid over a stretching sheet with chemical reaction. J Egypt Math Soc 2020;28:7. [CrossRef]